Ordered Mesoporous Spinel $LiMn_2O_4$ by a Soft-Chemical Process as a Cathode Material for Lithium-Ion Batteries

Jia-yan Luo, Yong-gang Wang, Huan-ming Xiong, and Yong-yao Xia*

Chemistry Department and Shanghai Key Laboratory of Molecular Catalysis and Innovative Materials, Fudan University, Shanghai 200433, China

Received May 25, 2007. Revised Manuscript Received July 2, 2007

Well-ordered mesoporous spinel-structured $LiMn_2O_4$ has been successfully prepared by annealing the lithiated mesoporous MnO_2 at a low temperature of 350 °C, in which the lithiated MnO_2 was obtained by the chemical lithiation of LiI with mesoporous MnO_2. Both low-temperature heat treatment and chemical lithiation processes could preserve the mesoporous structure of MnO_2. The ordered mesoporous $LiMn_2O_4$ shows high rate capability and excellent cycling ability as a cathode for lithium-ion batteries: it maintains 94% of its initial capacity after 500 cycles and keeps 80% of its reversible capacity at 0.1 C rate, even at 5 C rate.

Introduction

Lithium-ion batteries with both high-power and high-energy density are necessary for electric devices, especially for electric vehicles (EV) and other portable electric devices.[1−3] Although lithium-ion batteries are attractive power-storage devices with high-energy density, their power density is generally low because of the large polarization at high charge−discharge rates due to the low kinetics limited by the slow solid-state lithium-ion diffusion. It is well-established that the application of nanostructured electrode materials, especially the ordered mesoporous materials, is a desirable approach to improve the power density.[4−8] The ordered mesoporous materials have a relative large surface area, which decrease the current density per unit surface area; the thin wall can reduce the length of the diffusion path. Moreover, the well-ordered mesoporous materials can facilitate ionic motion more easily compared with conventional mesoporous materials in which the pores are randomly connected. Actually, many mesoporous electrode materials have recently been reported for the application of lithium-ion batteries.[9−14] It is well-known that the templating has been successfully used to prepare many mesoporous metal oxides, such as, Co_3O_4, NiO, Fe_2O_3, Cr_2O_3, etc. The typical process consists of the decomposition of the hydrated metal nitrate in the ordered mesoporous silica, then removal of the silica template by HF or NaOH solution.[15−20] By employing a similar synthesis process, we successfully prepared the mesoporous β-MnO_2 previously; it has high lithium electrochemical activity compared with the conventional crystal β-MnO_2 that is typically of electrochemical lithium inactivity.[21] However, it is very difficult to extend this synthetic methodology to prepare the ordered mesoporous lithium-ion intercalated compound because lithium precursor can react with the silica template if it is being directly prepared. Up to now, very few research works have been reported to prepare successfully the ordered mesoporous lithium-containing compounds. Zhao's group reported the mesoporous $LiTi_2(PO_4)_3$ using the poly (ethylene oxide)-poly (propylene oxide)−poly (ethylene oxide) triblock copolymer P123 as the template.[22] Zhou et al. reported the preparation of $Li_3Fe_2(PO_4)_3$ by employing cationic cetyltrimethylammonium chloride (CTMACl) as the template.[11−14] For these mesoporous electrode materials, the lithium ion iron/titanium phosphate can exclusively self-assembe, driven by the strong electrostatic interactions between the polycharged clusters and the polycharged surfactant micelles in solution, but it is

* To whom correspondence should be addressed. E-mail: yyxia@fudan.edu.cn. Fax: (+86)-21-55664177.

(1) Whittingham, M. S. *Chem. Rev.* **2004**, *104*, 4271.
(2) Scrosati, B. *Nature* **1995**, *373*, 557.
(3) Nelson, R. F. J. *Power Sources* **2001**, *92*, 2.
(4) Li, H.; Wu, X.; Chen, L. Q.; Huang, X. J. *Solid State Ionics* **2003**, *149*, 185.
(5) Li, H.; Shi, L. H.; Lu, W.; Huang, X. J.; Chen, L. Q. *J. Electrochem. Soc.* **2001**, *148*, A915.
(6) Zhang, S. S.; Ding, M. S.; Xu, K.; Allen, Jow, J., T. R. *Electrochem. Solid-State Lett.* **2001**, *4*, A206.
(7) Li, H.; Shi, L. H.; Wang, Q.; Chen, L. Q.; Huang, X. J. *Solid State Ionics* **2002**, *148*, 247.
(8) Doi, T.; Iriyama, Y.; Abe, T.; Ogumi, Z. *Chem. Mater.* **2005**, *17*, 1580.
(9) Liu, P.; Lee, S. H.; Tracy, C. E.; Yan, Y. F.; Turner, J. A. *Adv. Mater.* **2002**, *14*, 27.
(10) Kim, E.; Son, D.; Kim, T. C.; Cho, J.; Park, B.; Ryu, K. S.; Chang, S. H. *Angew. Chem., Int. Ed.* **2004**, *43*, 5987.
(11) Zhou, H. S.; Lin, D. L.; Hibino, M.; Honma, I. *Angew. Chem., Int. Ed.* **2005**, *44*, 797.
(12) Zhou, H. S.; Lin, D. L.; Honma, I. *Nat. Mater.* **2004**, *3*, 65.
(13) Zhou, H. S.; Zhu, S. M.; Hibino, M.; Honma, I.; Ichihara, M. *Adv. Mater.* **2003**, *15*, 2107.
(14) Zhu, S. M.; Zhou, H. S.; Miyoshi, T.; Hibino, M.; Honma, I.; Ichihara, M. *Adv. Mater.* **2004**, *16*, 2012.
(15) Tian, B. Z.; Liu, X. Y.; Yang, H. F.; Xie, S. H.; Yu, C. Z.; Tu, B.; Zhao, D. Y. *Adv. Mater.* **2003**, *15*, 1370.
(16) Wang, Y. Q.; Yang, C. M.; Schmidt, W.; Spliethoff, B.; Bill, E.; Schüth, F. *Adv. Mater.* **2005**, *17*, 5.
(17) Jiao, F.; Harrison, A.; Jumas, J. C.; Chadwick, A. V.; Kockelmann, W.; Bruce, P. G. *J. Am. Chem. Soc.* **2006**, *128*, 5468.
(18) Jiao, K.; Zhang, B.; Yue, B.; Ren, Y.; Liu, S. X.; Yan, S. Y.; Dickinson, C.; Zhou, W. Z.; He, H. Y. *Chem. Commun.* **2005**, 5618.
(19) Taguchi, A.; Schüth, F. *Microporous Mesoporous Mater.* **2005**, *77*, 1.
(20) Carreon, M. A.; Guliants, V. V. *Eur. J. Inorg. Chem.* **2005**, *1*, 27.
(21) Luo, J. Y.; Zhang, J. J.; Xia, Y. Y. *Chem. Mater.* **2006**, *18*, 5618.
(22) Tian, B. Z.; Liu, X. Y.; Tu, B.; Yu, C. Z.; Fan, J.; Wang, L. M.; Xie, S. H.; Stucky, G. D.; Zhao, D. Y. *Nat. Mater.* **2003**, *2*, 159.

10.1021/cm0714180 CCC: $37.00
Published on Web 08/17/2007

not available for the lithiated transition oxides, such as $LiCoO_2$, $LiMn_2O_4$, and $LiM_xNi_{1-x}NO_2$, which have been commercialized as cathode material for lithium-ion batteries. More recently, Bruce et al. reported a mesoporous low-temperature spinel structure $LiCoO_2$, rather than the common layered structure $LiCoO_2$, by a solid-state reaction of LiOH with mesoporous Co_3O_4 at a low temperature of 400 °C in which Co_3O_4 was prepared using mesoporous silica as a hard template.[23] The spinel structure $LiMn_2O_4$ has been widely studied as a promising cathode material for lithium-ion batteries, especially for electric vehicle applications because they are cheaper, less toxic, and safer in the overcharged state.[24−28] However, the ordered mesoporous $LiMn_2O_4$ cannot be directly prepared by the same process as low-temperature $LiCoO_2$, via a solid-state reaction of lithium salt and mesoporous MnO_x at low temperature because the typical temperature for the formation of $LiMn_2O_4$ by a solid-state reaction should be over 600 °C or more, but the high-temperature treatment will cause the collapse of the self-ordered mesoporous structure.[11,12] Therefor, it would be of great interest, but a big challenge, to prepare the ordered mesoporous $LiMn_2O_4$ electrode material for high-power and high-energy density lithium-ion batteries.

In the present work, we prepared successfully a well-ordered mesoporous spinel-structured $LiMn_2O_4$ by annealing the lithiated mesoporous MnO_2 at a low temperature of 350 °C in which the lithiated MnO_2 was obtained by the chemical lithiation of LiI with mesoporous MnO_2. Both low-temperature heat treatment and chemical lithiation process could preserve the mesoporous structure of MnO_2. The ordered mesoporous $LiMn_2O_4$ shows high rate capability and excellent cycling ability as a cathode for lithium-ion batteries.

Experimental Section

Mesoporous silica KIT-6 was prepared according to the reported procedure.[29] The mesoporous MnO_2 with regular mesoporous was synthesized using mesoporous silica KIT-6 as a template.[21] A typical synthesis of mesoporous $LiMn_2O_4$ was as follows: 6 g $Mn(NO_3)_2 \cdot 4H_2O$ (50%) was dissolved in 25 mL ethanol, and then 1 g KIT-6 was added to the above solution. The mixture was stirred overnight, and then a powder specimen was obtained. The solid was then calcined in a muffle furnace with a heating rate of 1 °C /min from room temperature to 350 °C and then maintained at 350 °C for 5 h followed by the solution etching of the silica framework by a 2 M NaOH solution. Centrifugation was preferred to separate the final products. Washing with distilled water and ethanol and then dried at 80 °C were also performed to obtain the MnO_2 with an ordered mesoporous structure. LiI (0.1675 g) was dissolved in acetonitrile (25 mL) and then stirred at room temperature until the solution became clear. As-prepared mesoporous MnO_2 (0.145 g) was then added to the solution. The suspension was heated to 70 °C, kept under reflux for 12 h, centrifugated, washed several times with acetrotrile, and then calcined under a vacuum at 350 °C for 2 h to get the final products. For comparison, a lithium-rich spinel $Li_{1.06}Mn_2O_4$ was also prepared by a solid-state reaction of MnO_2 and LiOH (lithium/manganese = 0.53 in molar ratio) at 470 °C for 12 h and 750 °C for 12 h in air.

Scheme 1. Illustration of the Synthesis Procedure

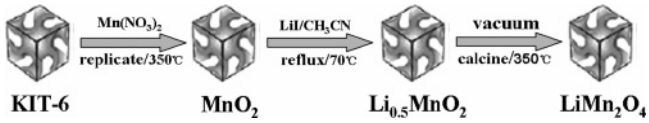

The chemical composition of the products was obtained by inductively coupled plasma (ICP) analysis. The manganese valence in $LiMn_2O_4$ was calculated by analysis according to Kozawa's method.[30] $LiMn_2O_4$ was dissolved in an $FeSO_4/H_2SO_4$ solution. The oxidation of manganese can be determined by titrating the excess $FeSO_4$ solution with standard $KMnO_4$ solution.

The as-prepared samples were characterized by small-angle and wide-angle XRD (Rigaku D/MAX-IIA X-ray generator, Cu Kα radiation), TEM, HRTEM (JOEL JEM-2010 electron microscope), and N_2 adsorption (Micromeritics Tristar 3000).

The electrochemical test was characterized in a CR2016-type coin cell. Metallic lithium was used as the negative electrode. The working electrode was fabricated by compressing a mixture of the active materials (mesoporous $LiMn_2O_4$), conductive material (acetylene black), and binder (polytetrafluoroethylene) in a weight ratio of 80:15:5 onto an aluminum grid at 10 Mpa. The electrodes were punched in the form of disks, typically with a diameter of 12 mm. The typical mass load of the active material is about 10 mg/cm^2. The electrode was dried at 120 °C for 12 h before assembly. The cell assembly was operated in a glovebox filled with pure argon. The electrolyte solution was 1 M $LiPF_6$/ethylene carbonate (EC)/diethyl carbonate (DMC)/ethyl methyl carbonate (EMC) (1:1:1 by volume). The electrochemical measurements were performed using an Arbin charge−discharge unit at room temperature. Lithium insertion into the $LiMn_2O_4$ electrode was referred to as discharge and extraction as charge.

Results and Discussion

The preparation of mesoporous $LiMn_2O_4$ can be briefly described by the following process, as shown in Scheme 1, which includes (1) the use of the ordered mesostructured KIT-6 as a template to synthesize ordered mesoporous MnO_2 using a nanocasting method, (2) lithiating mesoporous MnO_2 with LiI under refluxing in acetonitrile to get $Li_{0.5}MnO_2$,[31,32] and (3) annealing the $Li_{0.5}MnO_2$ under a vacuum at a low temperature of 350 °C to transform to the spinel $LiMn_2O_4$, where the vacuum condition prevents the oxidation of $Li_{0.5}MnO_2$, transforming sluggishly to oxygen-rich spinel $Li_2Mn_4O_9$.[33,34]

Figure 1 shows the small-angle X-ray diffraction (XRD) patterns of mesoporous MnO_2 and $LiMn_2O_4$. The characteristic diffraction peaks index as (211), (220), and (332) of

(23) Jiao, F.; Shaju, K. M.; Bruce, P. G. *Angew. Chem., Int. Ed*. **2005**, *44*, 6050.
(24) Tarascon, J. M.; Mckinnon, W. R.; Coowar, F.; Browmer, T. N.; Amatucci, G.; Guymard, D. *J. Electrochem. Soc*. **1994**, *141*, 1421.
(25) Xia, Y. Y.; Yoshio, M. *J. Electrochem. Soc*. **1996**, *143*, 825.
(26) Xia, Y. Y.; Yoshio, M. *J. Electrochem. Soc*. **1997**, *144*, 4186.
(27) Xia, Y. Y.; Zhou, Y. H.; Yoshio, M. *J. Electrochem. Soc*. **1997**, *144*, 4186.
(28) Xia, Y. Y.; Sakai, T.; Fujieda, T.; Yang, X. Q.; Sun, X.; Ma, Z. F.; McBreen, J.; Yoshio, M. *J. Electrochem. Soc*. **2001**, *148*, A723.
(29) Kleitz, F.; Choi, S. H.; Ryoo, R. *Chem. Commun*. **2003**, *17*, 2136.
(30) Kozawa, A. *Memo. Fac. Eng. Nogoya Univ*. **1959**, *11*, 243.
(31) Pistoia, G.; Antonini, A.; Zane, D.; Pasquali, M. *J. Power Sources* **1995**, *56*, 37.
(32) Thackray, M. M.; Rossouw, M. H.; Gummow, R. J.; Liles, D. C.; Pearce, K.; De-Kock, A.; David, W. I. F.; Hull, S. *Electrochim. Acta* **1993**, *38*, 1259.
(33) Luo, J. Y.; Li, X. L.; Xia, Y. Y. *Electrochim. Acta* **2007**, *52*, 4525.
(34) Luo, J. Y.; Cheng, L.; Xia, Y. Y. *Electrochim. Commun*. **2007**, *9*, 1404.

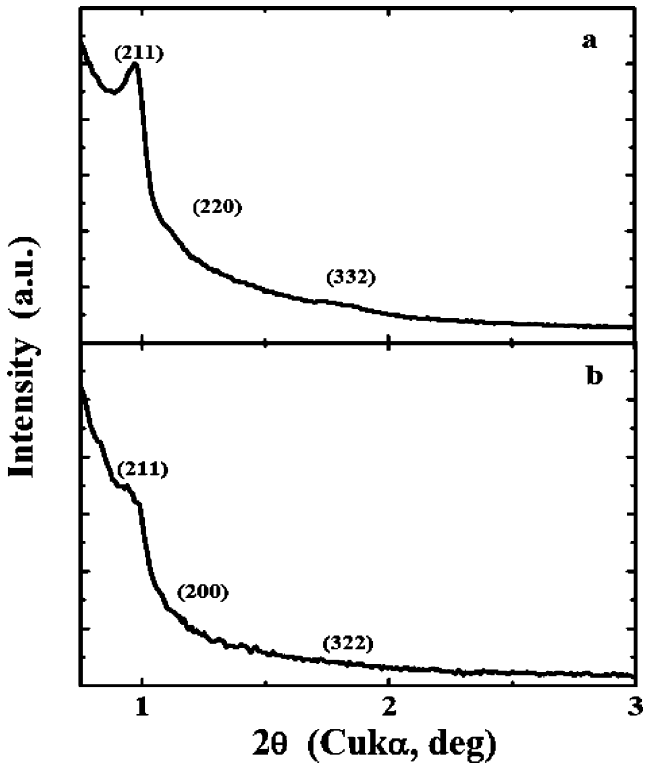

Figure 1. Small-angle X-ray diffraction patterns of (a) as-prepared mesoporous MnO_2, and (b) mesoporous $LiMn_2O_4$.

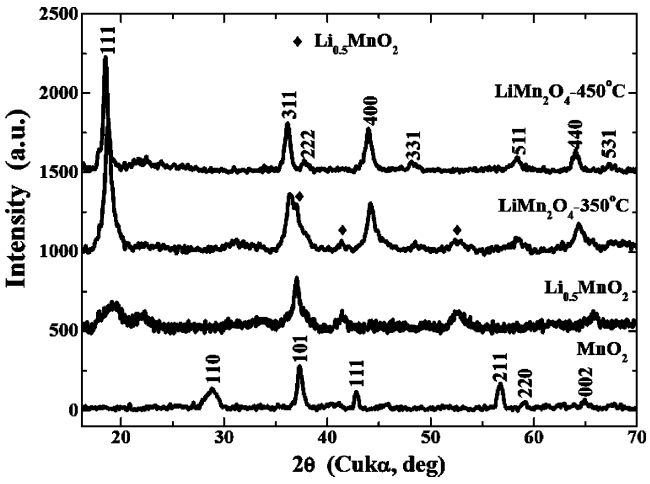

Figure 2. XRD patterns of the as-prepared compounds (a) MnO_2, (b) chemical lithiated MnO_2, chemical lithiated MnO_2 heat treated (c) at 350 °C under a vacuum for 2h and (d) at 450 °C under a vacuum for 2 h.

the Ia3d cubic, the mesoporous structure of which can be observed, although the higher-order reflections are not very pronounced or well resolved. The appearance of small-angle X-ray diffraction peaks corresponding to an Ia3d cubic structure for mesoporous $LiMn_2O_4$ indicates that the mesostructure is preserved upon chemical lithiation and heat-treatment processes, although the superstructure has contracted slightly, as evidenced by a slight shift of the small-angle XRD peaks toward a larger angle. The phase composition and structure of the mesoporous MnO_2, $LiMn_2O_4$, and the intermediate product were examined by the wide-angle powder XRD and chemical analysis, and the XRD patterns are given in Figure 2. The XRD patterns of mesoporous MnO_2 can be indexed to the tetragonal phase of β-MnO_2 (space group: $P4_2/mnm$) narrowest (1 × 1)

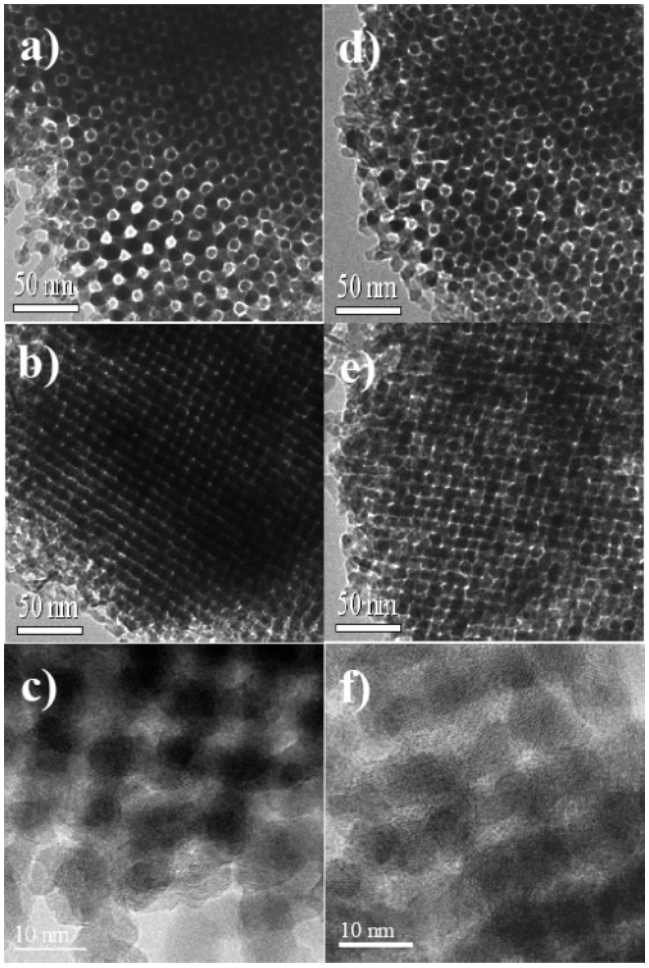

Figure 3. TEM images of mesoporous MnO_2 along the a) [111] and b) [531] directions, and c) high-resolution image of mesoporous MnO_2. TEM images of mesoporous $LiMn_2O_4$ along the a) [111] and b) [531] directions, and c) high-resolution image of mesoporous $LiMn_2O_4$.

channels. The chemical lithated MnO_2 is characterized by the ramsdellite lithiated MnO_2 as evidenced by the peaks of $2\theta = 20.1$, 37.2, 41.3, and 52.5°, with a chemical composition of $Li_{0.53}MnO_2$.[32] For the mesoporous $LiMn_2O_4$ obtained by heat-treating the lithiated MnO_2 at 350 °C under a vacuum, almost all of the diffraction peaks of the wide-angle XRD pattern can been indexed to a face-centered cubic $LiMn_2O_4$ structure (space group: $Fd\bar{3}\,m(227)$), which is in good agreement with that of the standard values (JCPDS No. 89−1026). The broading of the peaks in the wide-angle XRD pattern indicates that the component crystallites are of nanoscare character. Very small peaks were observed at 41.3 and 52.5°, indicating that the resultant compound contained a small amount of the intermediate compound between the MnO_2 and the $LiMn_2O_4$ spinel phases, lithiated MnO_2. Moreover, the chemical composition of the product by inductively coupled plasma (ICP) analysis is lithium/manganese = 0.53 in molar ratio, and the average manganese valence in $LiMn_2O_4$ determined by chemical titration is 3.60. When the calcining temperature was increased to 450 °C, pure spinel $LiMn_2O_4$ phase can be obtained with the chemical formula $Li_{1.05}Mn_2O_{4.12}$ but resulting in a collapse of the mesoporous nanostructure (Supporting Information).

Figure 3 shows transmission electron microscopic (TEM) images of mesoporous MnO_2 and $LiMn_2O_4$. The replication

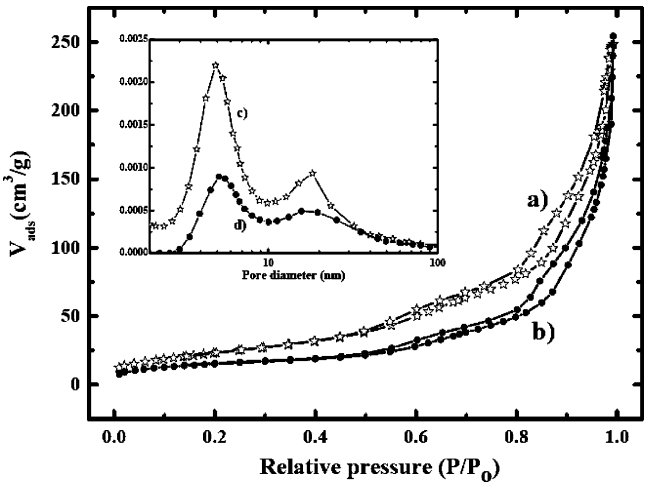

Figure 4. Nitrogen asorption and desorption isotherms for a) mesoporous MnO_2 and b) mesoporous $LiMn_2O_4$. The inset shows the pore size distribution for c) mesoporous MnO_2 and d) mesoporous $LiMn_2O_4$.

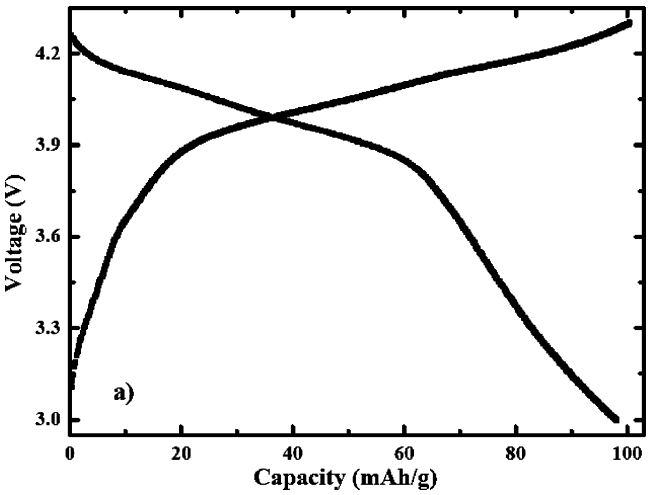

Figure 5. Typical charge/discharge curves of the mesoporous $LiMn_2O_4$ between voltage limits of 3.0 and 4.3 V at a current rate of 1 C.

of the KIT-6 silica by MnO_2 can also be directly observed in TEM images taken along different axes in parts a−c of Figure 3. The hexagonal image contrast pattern in part a of Figure 2, where the mesoporous channels are seen as bright contrast, indicating that the image is viewed down the [111] zone axis of the KIT-6 related cubic unit cell, and the cell dimension is similar to that of KIT-6, which is in good agreement with the small-angle XRD in Figure 1. As for the mesoporous $LiMn_2O_4$ formed from MnO_2, TEM data for this material are shown in parts d−f of Figure 3. It is clear that the cubic mesoporous morphology of MnO_2 is preserved upon chemical lithiation and heat-treatment processes, and the morphology extends throughout the sample. There was no difference between the wall thickness of the mesoporous MnO_2 and $LiMn_2O_4$ by comparing parts d and f of Figure 3.

The nitrogen-adsorption isotherms of the as-synthesized mesoporous MnO_2 and $LiMn_2O_4$ powder are shown in Figure 4. The Brunauer−Emmett−Teller (BET) surface areas are 84 and 55 m^2g^{-1} for as-synthesized mesoporous MnO_2 and $LiMn_2O_4$, respectively. Although the BET surface area of mesoporous $LiMn_2O_4$ was decreased by ∼30% compared with that of the mesoporous MnO_2, both adsorption isotherm curves have a well-defined step for the relative pressure P_s/P_0 ranging from 0.6 to 0.8 as the typical IV classification with a clear H_1-type hysteretic loop, which is characteristic of mesoporous materials. Therefor, it can be concluded that the chemical lithiation and heat-treatment processes do not lead to a collapse of the mesostruture, which is also evidenced by the well-devolved TEM images. The shape of the pore size distribution curves for mesoporous MnO_2 and $LiMn_2O_4$ was almost the same, with the peaks centering at 4.9 and 18 nm, whereas the former reflects the minimum wall thickness of KIT-6 and the latter is corresponding to the wall junctions in KIT-6 or to the pores between the particles, except for the decreased accumulated pore volume, which is in good accordance with the BET area measurement. The decease of the BET surface area is believed to be caused by an amorphous-crystalline transition during heat treatment, and the high thermal stability makes the walls of the mesopores sinter.

Figure 5 displays the charge/discharge curves for the electrode of mesoporous $LiMn_2O_4$, recorded over a potential range between 3.0 and 4.3 V at a rate of 1 C (where C corresponds to complete discharge of the theoretical capacity in 1 h). The discharge curve of mesoporous $LiMn_2O_4$ presents two undistinguished plateaus, which are the charge/discharge signature of the lithium-rich spinel and a sloping part. The flat part of the charge/discharge of mesoporous $LiMn_2O_4$ is about 70 mAh/g, which was much less than that of conventional or commercially available $LiMn_2O_4$, and the sloping part is about 25 mAh/g. The sloping part is generally considered as capacitive behavior of the surface storage of lithium, which has been widely observed in high BET surface area mesoporous and other nanostructured materials.[11,21,35−37] In the current case, partial capacity of the sloping part is also contributed to by the impurity of lithiated MnO_2. Typical discharge capacity of the lithiated MnO_2 in the examined voltage region between 3.0 and 4.3 V is about 50 mAh/g. When the lithiated mesoporous MnO_2 was calcined at 450 °C under a vacuum for 2 h, the resulting $LiMn_2O_4$ exhibits much better charge/discharge behavior, displaying a higher discharge voltage and a longer plateau of about 105 mAh/g (Supporting Information).

Nevertheless, as the calcining temperature was increased to 450 °C, although the crystal spinel $LiMn_2O_4$ phase can be easily obtained, the ordered mesoporous nanostructure was destroyed during its production by heating. Moreover, there is nearly no step for the relative pressure P_s/P_0 ranging from 0.6 to 0.8, with a clear H_1-type hysteretic loop in the nitrogen-adsorption isotherms curves (Supporting Information). The collapse of the mesostructure is believed to be caused by an amorphous-crystalline transition during heating. So, the mesoporous morphology can be preserved only under a relative low-calcining temperature, even though the crystallinity of mesoporous $LiMn_2O_4$ is not perfect. It has been demonstrated that the relative large surface area of ordered

(35) Gao, X.; Zhu, H.; Pan, G.; Ye, S.; Lan, Y.; Wu, F.; Song, D. *J. Phys. Chem. B* **2004**, *108*, 2826.
(36) Wagemaker, M.; Kearley, G. J.; Vanwell, A. A.; Mutka, H.; Mulder, F. M. *J. Am. Chem. Soc*. **2003**, *125*, 840.
(37) Armstrong, A. R.; Armstrong, G.; Canales, J.; Bruce, P. G. *Angew. Chem., Int. Ed*. **2004**, *43*, 2286.

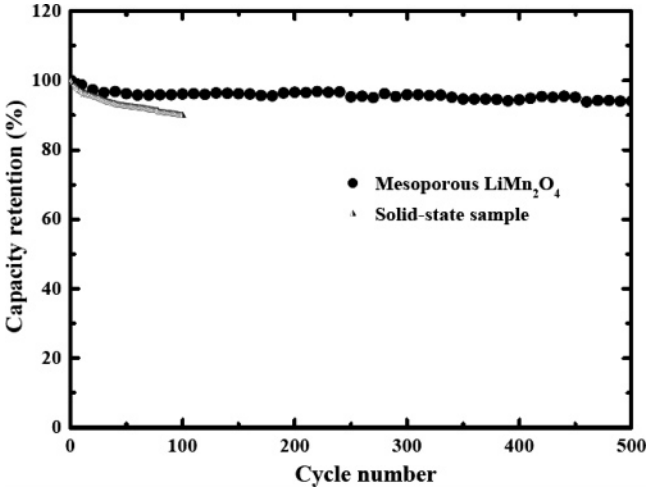

Figure 6. Variation of discharge capacities versus cycle number for mesoporous $LiMn_2O_4$ and solid-state reaction $LiMn_2O_4$ cycled between voltage limits of 3.0 and 4.3 V at a current rate 1 C.

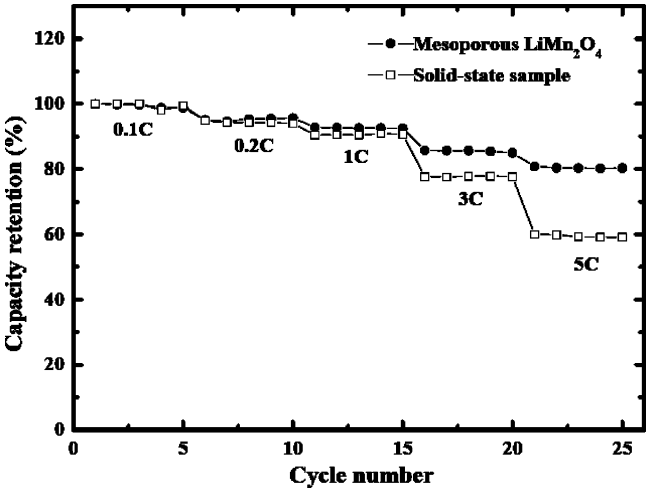

Figure 7. Variation in discharge capacities versus cycle number for mesoporous $LiMn_2O_4$ and solid-state reaction $LiMn_2O_4$ cycled at 0.1, 0.5, 1, 3, and 5 C between voltage limits of 3.0 and 4.3 V.

mesoporous materials can decrease the current density per unit surface area, and the thin wall can reduce the length of the diffusion path. Moreover, the well-ordered mesoporous materials can facilitate ionic motion more easily, compared with conventional mesoporous materials in which the pores are randomly connected. As a result, improved cycling ability and rate capability of the as-synthesized the mesoporous $LiMn_2O_4$ electrode would be expected.

Figure 6 shows the cycle performance of mesoporous $LiMn_2O_4$ and solid-state reaction $LiMn_2O_4$ electrodes between potential limits of 3.0 and 4.3 V at a rate of 1 C. As-synthesized mesoporous $LiMn_2O_4$ exhibits excellent cycling performance. It shows a slow capacity that fades upon cycling, with an average capacity loss of no more than 0.04% per cycle on the first 100 cycles and then a decrease to even lower than 0.005% during further cycling. Mesoporous $LiMn_2O_4$ maintains 94% of its initial capacity after 500 cycles. To the best of our knowledge, it is the best cycling life of any reported $LiMn_2O_4$, whereas solid-state reaction $LiMn_2O_4$ only keeps 90% of the initial capacity for the 100 charge/discharge cycles. The excellent cycling ability of the mesoporous $LiMn_2O_4$ can be ascribed to the fact that the ordered mesoporous structure would act as a buffer layer to alleviate the volume expansion of the electrode during lithiation/delithiation. The rate capability performance, especially at a high rate, is another important aspect for the application of manganese-based spinel cathodes for EV/HEV power sources besides the cycling performance. Figure 7 shows the discharge capacity of mesoporous $LiMn_2O_4$ and solid-state reaction $LiMn_2O_4$ during cycling at different current rates, varying from 0.1 to 5 C. At 5 C, it keeps about 80% of its capacity compared with that at a rate of 0.1 C, which is much higher than that of the solid-state reaction $LiMn_2O_4$ at the same rate (about 60% higher). The result demonstrates that the role of the mesoporous structure of $LiMn_2O_4$ may facilitate the fast transport and intercalation kinetics of lithium ions: the ordered arrangement guarantees that a rapid charge−discharge process will be complete in a very short time, resulting in a high specific capacity, even at a high charge−discharge current.

Conclusion

In summary, we have developed a soft-chemical method for the successful synthesis of mesoporous $LiMn_2O_4$ by annealing the lithiated mesoporous MnO_2 at a low temperature of 350 °C. Both low-temperature heat treatment and chemical lithiation processes could preserve the mesoporous structure of MnO_2, but the high-temperature treatment results in a partial collapse of the mesoporous nanostructure. As-synthesized ordered mesoporous $LiMn_2O_4$ shows high rate capability and excellent cycling ability as a cathode material for lithium-ion batteries. The role of the mesoporous structure of $LiMn_2O_4$ may facilitate the fast transport and intercalation kinetics of lithium ions. The soft chemical method described in the present work could be used to develop other nanostructured $LiMn_2O_4$, such as, nanorod, nanowire, nanobelt, nanotube, urchin-like nanostructure, hollow spheres, and so on. Besides, this synthetic methodology can be easily extended to the preparation of the ordered mesoporous lithium-ion intercalated, such as, $Li_xV_2O_5$, $LiCr_3O_8$, $LiFePO_4$, $LiMnPO_4$, $LiCoPO_4$, and so on by annealing the lithiated corresponding mesoporous oxides and phosphate. Furthermore, the strategy presents a new possibility for the synthesis of various nanostructured mixed metal oxides and phosphate.

Acknowledgment. This work was partially supported by the National Natural Science Foundation of China (No. 20633040) and the 863 program of China (No. 2006AA05Z218).

Supporting Information Available: TEM images of $LiMn_2O_4$, a graph nitrogen asorption and desorption isotherms of $LiMn_2O_4$, and a curves of liathiated MnO_2 under various conditions. This material is available free of charge via the Internet at http://pubs.acs.org.

CM0714180